Nig. J. Pure & Appl. Sci. Vol. 33 (Issue 2, 2020)
e-ISSN 2756-4045

www.njpas.com.ng

http://dx.doi.org/10.48198/NJPAS/20.B01

Investigation of the Optical and Dielectric Behaviour of SnO_2-CuO Mixed Oxides Thin Films

[1,2] *Animasahun, L.O., [1]Taleatu, B.A., [2]Bolarinwa, H.S., [3]Egunjobi, A.I., [4]Fasasi, A.Y., [1]Eleruja, M.A.

[1]Department of Physics and Engineering Physics, Obafemi Awolowo University, Ile Ife, Nigeria
[2]Department of Physics, Electronics and Earth Sciences, Fountain University Osogbo, Nigeria
[3]Department of Physics, Federal University of Agriculture, Abeokuta, Ogun State, Nigeria.
[4]Center for Energy Research and Development, Obafemi Awolowo University, Ile Ife, Nigeria

ABSTRACT

The effects of CuO on the optical and dielectric properties of SnO_2 thin film were studied to achieve improved light photon absorption and conversion. The films were deposited using airblast chemical spray pyrolysis. Rutherford Backscattering Spectrometric analysis using the Windows SIMNRA software gave the compositions of as-deposited and annealed films and their thicknesses. The optical and dielectric parameters were evaluated from the transmittance data obtained from UV – Visible spectrophotometer. The optical band gap of as-deposited SnO_2-CuO film was evaluated to be 3.4 eV. The value of Urbach tail width of the as-deposited mixed oxide is higher (296 meV) compared to that of the annealed (252 meV) indicating the presence of more disordered states in the as-deposited film. The analysis also showed that the presence of CuO in the matrix of SnO_2 led to a decrease in optical bandgap, refractive index, and by extension dielectric constants of SnO_2. Our investigation led to the conclusion that the addition of CuO into SnO_2 increased its electromagnetic photon absorption and also delay its speed thereby enhancing photon interaction with free charge carriers in the mixed oxide film. We opined that the mixed oxide will perform better in photocatalysis, photodegradation of pollutants and other light-harvesting applications since the CuO inclusion has extended its absorption edge towards the visible light range.

Keywords: photodegradation, light-harvesting, optical bandgap, refractive index, dielectric constants, Urbach tail, thin film

Introduction

Two of the prominent challenges of this generation are the quest for clean and sustainable energy and the need to reduce environmental pollutions and the effects of climate change. The best approaches to solving these problems have been the need to improve our efficiency in tapping renewable energy sources most importantly solar energy. While this will reduce our dependence on fossil sources which is good, the need for efficient detection and safe photodegradation of pollutants is also fundamental to solving these problems. These approaches require materials that could harvest the bulk of electromagnetic photons from the sun. One of such materials that have found wide applications in solar energy conversion, photodegradation of pollutants, gas sensing and

Corresponding Author: **Animasahun, L.O.**
Department of Physics and Engineering Physics, Obafemi Awolowo University, Ile Ife, Nigeria
Department of Physics, Electronics and Earth Sciences, Fountain University Osogbo, Nigeria
Email: luqman.animasahun@gmail.com, ayfasasi@gmail.com

photocatalysis is tin (IV) oxide, SnO_2. The popularity of SnO_2 in photocatalysis and photodegradation of environmental pollutants could best be demonstrated by the number of recent publications on the subject (Uddin *et al.*, 2012; Ayadi *et al.*, 2019; Sujatha *et al.*, 2019; Yu *et al.*, 2019; Magdalane *et al.*, 2019; Navidpour *et al.*, 2019; Ullah *et al.*, 2020; Karpuraranjith *et al.*, 2020). It is one of the metal oxide materials that possess high electrical conductivity with optical transparency and thus establishes itself as an important component for optoelectronic applications such as flat panel displays, solar cells, photodetectors, light-emitting diodes (LEDs) and transistors (Bau *et al.*, 1997; Tsay and Liang, 2015; Yildirin *et al.*, 2014). It is also the most commonly used metal oxide gas sensing material (Batzill *et al.*, 2005; Liu *et al.*, 2012; Patil *et al.*, 2012). Besides other qualities, for any light-harvesting, photocatalysis and photodegradation applications one of the most desirable properties in a material is its ability to absorb a considerable amount of electromagnetic light photons. This is a downside for SnO_2 as for many other metal oxides: zinc oxide (ZnO), titanium oxide (TiO_2), etc. Despite its favourable electronic structure, catalytic activity, thermodynamic stability and suitable physicochemical properties, its bandgap of approximately 3.9 eV indicates that it can only absorb within the ultraviolet region of the electromagnetic spectrum (Animasahun *et al*., 2019). Hence its excitation would require a UV source which is not usually safe for human exposure. For this reason, more recent works on photodegradation and photocatalytic applications of SnO_2 have been focused on doped/composite/mixed/solid solutions of this oxide such as Cu: SnO_2 (Babu *et al.*, 2017; Sathishkumar and Geethalakshmi, 2020), MoS_2-SnO_2 core-shell microsphere (Yu-Chen *et al.*, 2020), SnO_2-CNTs nanoarchitecture (Karpura ranjith *et al.*, 2020), Ni-doped SnO_2-SnS_2 heterojunctions (Chen *et al.*, 2019), SnO_2/TiO_2 nanostructure (Magdalane *et al.*, 2019), vanadium-doped SnO_2 (Letifi *et al.*, 2019), cerium-doped SnO_2 (Ayadi *et al.*, 2019), and so on. Mixed or composite oxides have been explored for a lot of other applications such as electrocatalysts for fuel cells (Garino, *et al.*, 2016), as an electron transporting layer in perovskite solar cells (Mahmood *et al.*, 2015), photocatalyst for hydrogen productions (Sinatra *et al.*, 2015). Many kinds of research have been carried out on properties and applications of SnO_2-CuO/Cu: SnO_2 composite oxides in recent times such as ferromagnetic properties (Akbar *et al.*, 2020), optical and dielectric properties (Jahnavi *et al.*, 2020), photoluminescence (Nachiar and Muthukumaran, 2019), electronic and optical properties (Shao and Zhang, 2019), electron dosimetric properties (Bhadane *et al.*, 2019), and gas sensing behaviour (Choi *et al.*, 2013; Somjaijaroen *et al* 2019). However, the effects of CuO on optical and dielectric properties of SnO_2 have not been comprehensively investigated. Hence, this work was carried out to fill this gap and deepen the knowledge of the scientific community on the effects of CuO on the general optical and dielectric properties of SnO_2 and most importantly the increased photon absorption observed in SnO_2-CuO system. Thin films of the SnO_2-CuO system was deposited via chemical spray pyrolysis using air-blast atomization. Our method yielded quality films with excellent adhesion to the substrate.

Materials and Methods

The precursor solutions were prepared from tin II chloride dihydrate purchased from Sigma Aldrich, copper II nitrate trihydrate from Bosch, ethanol and distilled water. The salts were of analytical grade and were used as purchased without any further purification. All the solutions were 0.1 M in concentrations. 0.1 M solution of tin II chloride dihydrate ($SnO_2 \cdot 2H_2O$) was prepared by dissolving 2.10g of the salt in 100ml of ethanol and distilled water. 0.1 M solution of copper II nitrate trihydrate ($Cu(NO_3)_2 \cdot 3H_2O$) was prepared by dissolving 1.21 g of the salt in 100ml of ethanol and distilled water.

The mixtures were thoroughly stirred using a magnetic stirrer to form a clear homogeneous solution. In a typical deposition, SnO_2 – CuO composite films were produced by mixing the precursor solutions of both Sn^{2+} and Cu^{2+} in 70 to 30 % volume ratio respectively before spraying. The glass substrates were precleaned in dilute hydrochloric acid, alcohol and distilled water and briefly dried on the electric hot plate. The spraying (Ayadi *et al.*, 2019 and Animasahun *et al*., 2019) was carried out using a suction-based Master Airbrush (USA) at a nozzle – to – substrate distance of 23 cm and substrate temperature of 350 ± 5 °C. The samples were annealed in the open-end tubular furnace for an adequate supply of oxygen at 500 °C.

Rutherford Backscattering Spectroscopic mode of the Pelletron Tandem Accelerator at the Centre for Energy Research and Development was used to investigate the stoichiometric compositions and thickness of the films. The RBS experiment was performed using 2.2 MeV $^4He^{2+}$ ion beam as projectile ions with scattering angle of 165o, detector resolution of 12 KeV and the current range of 20 – 60 nA at a constant charge of 20 μC. The RBS spectra were fitted with Windows SIMNRA 6.06 software. The optical properties of the films were investigated with the Stellanet UV – Visible spectrophotometer (EP2000) covering ultra-violet to near-infrared frequencies. The optical and dielectric parameters were evaluated from the transmittance data.

Results

The results of the simulations gave the relative amounts of each element and the film thickness (in atoms/cm^2) of each sample. The atomic density of the film (in atoms/cm^3) is given in equation 1, while the thickness in nanometer is calculated by dividing the thickness (in atoms/cm^2) from the RBS analysis by the atomic density (in atoms/cm^3) as given in equation 2.

$$Atomic\ density = \frac{\rho N_a}{M} \qquad 1a$$

$$Thickness\ (nm) = \frac{thickness\ (atoms/cm^2)\times 10^7}{atomic\ density\ (atoms/cm^3)} \qquad 1b$$

where ρ is the density of element, Na is the Avogadro's number and M is the molecular mass of the element. For a compound or a composite such as metal oxide, the atomic density is calculated by multiplying the atomic density of each element by its fractional amount in the material and adding them together. The RBS spectra are shown in Figure 1 and the thickness and compositions of the films are presented in Table 1.

Optical characterizations

The optical band gap E_g is calculated from Tauc's relation given in equation 2 where α denotes the

$$(\alpha hv) = B(hv - E_g)^n \qquad 2$$

absorption coefficient obtained by the relation $\alpha = 1/d(ln1/T)$. The Tauc's plots were based on n = 2 for the indirect allowed transition. B is an empirical constant and hv is the photon energy in electron-volt (eV). Values of $(\alpha hv)^{1/2}$ were plotted against hv and energy bandgap E_g was estimated by extrapolating the linear part of the graph to the photon energy axis at $(\alpha hv)^{1/2} = 0$. The transmittance plot Figure 2(a) and Tauc's for optical band gaps Figure 2(b) of both annealed and as-deposited have been included.

Urbach Tail Width

The exponential tail found in the band structures appears because disordered and amorphous materials produced localized states extended in the bandgap. For low photon energy, it is assumed that the spectral dependence of the absorption edge follows the empirical Urbach rule given by

$$\propto (v) = \alpha_o exp\left(\frac{hv}{E_t}\right) \qquad 3$$

where α_o is a constant, hv is the photon energy and E_t denotes the width of the tail of localized states in the bandgap (Urbach energy). By plotting ln(α) against the photon energy hv, a linear fit was established in the linear portions of the curves as

shown in Figure 3. The Urbach energy E_t is the inverse of the slope of the linear fit.

Table 1: Result of RBS analysis showing the composition and thickness of films

FILMS	COMPOSITION	THICKNESS (*d*) (nm)
SnO_2-CuO (70:30) (as-deposited)	$Sn_{0.11}0_{0.88}Cu_{0.01}$	547.62
SnO_2-CuO (70:30) (annealed)	$Sn_{0.11}0_{0.87}Cu_{0.02}$	669.34

Refractive Index Dispersion

The reflectance was calculated from the transmittance data obtained from the UV-Visible spectrophotometer using the relation in equation 4 where R is the reflectance, T is the transmittance and d is the film thickness.

$$R = 1 - [Texp(\alpha d)]^{1/2} \quad (4)$$

Using the reflectance data derived from transmission data of both the as-deposited and annealed films and employing the relationship between reflectance, refractive index and skin depth presented in equation 5, the variation in the refractive index and skin depth as a function of the photon wavelength was obtained. The results are presented in Figure 4 and 5.

$$n = \frac{1+\sqrt{R}}{1-\sqrt{R}} \quad \text{and} \quad k = \frac{\alpha\lambda}{4\pi} \quad (5)$$

Optical Conductivity

The optical conductivity is a measure of the conductivity at various frequencies, unlike the static electrical conductivity which gives conductivity at a fixed frequency. It is a function of the absorption coefficient, refractive index, skin depth and speed of light c, as presented in equation (6).

$$\sigma_{opt} = \frac{\alpha nc}{4\pi k} \quad (6)$$

The plot of optical conductivities versus wavelengths for as-deposited and annealed films are shown in Figure 6.

Dielectric Constants

The dielectric constants of a material affect the speed of electromagnetic waves inside it. As the refractive index, it is a complex function. The relationship between both the real and imaginary components of the two and the dissipation factor are given in equations (7), (8) and (9).

$$\varepsilon' = n^2 - k^2 \quad (7)$$

$$\varepsilon'' = 2nk \quad (8)$$

$$tan\delta = \frac{\varepsilon''}{\varepsilon'} \quad (9)$$

$\varepsilon'$is the real and $\varepsilon''$is the imaginary parts of the dielectric function while δ is the dissipation factor or loss tangent. The plots ε', $\varepsilon''$and $tan\delta$ against wavelength are shown in Figures 7 (a), (b) and (c). Also, the high-frequency dielectric constant ε_∞ was evaluated using the relation in equation (10).

$$\varepsilon' = n^2 = \varepsilon_\infty - \left(\frac{e^2}{\pi c^2}\right)\left(\frac{N_c}{m^*}\right)\lambda^2 \quad (10)$$

where e is the electronic charge, c is the speed of light, N_c is the carrier density and m^* is the effective mass of the carrier. From the plot of n^2 against λ^2, the intersection at $\lambda^2 = 0$ for the linear part of the curve at higher wavelength gave the high-frequency dielectric constant ε_∞ for the as-deposited and annealed films. This is presented in Figure 7 (d).

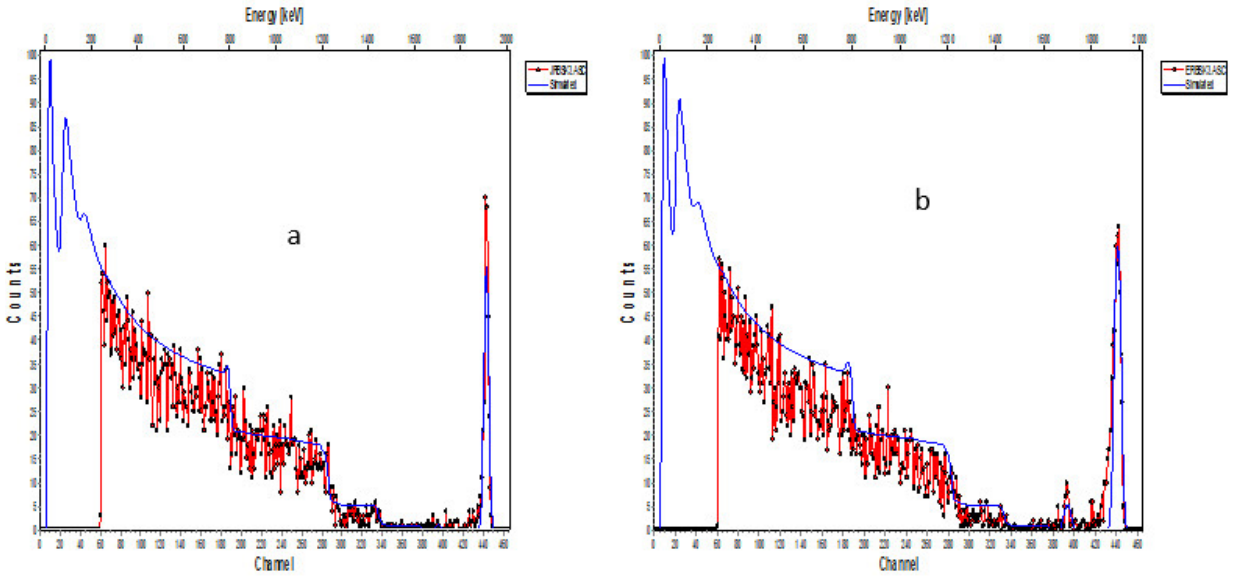

Figure 1: RBS spectrum of SnO_2-CuO(a) as-deposited (b) annealed at 500 ^oC

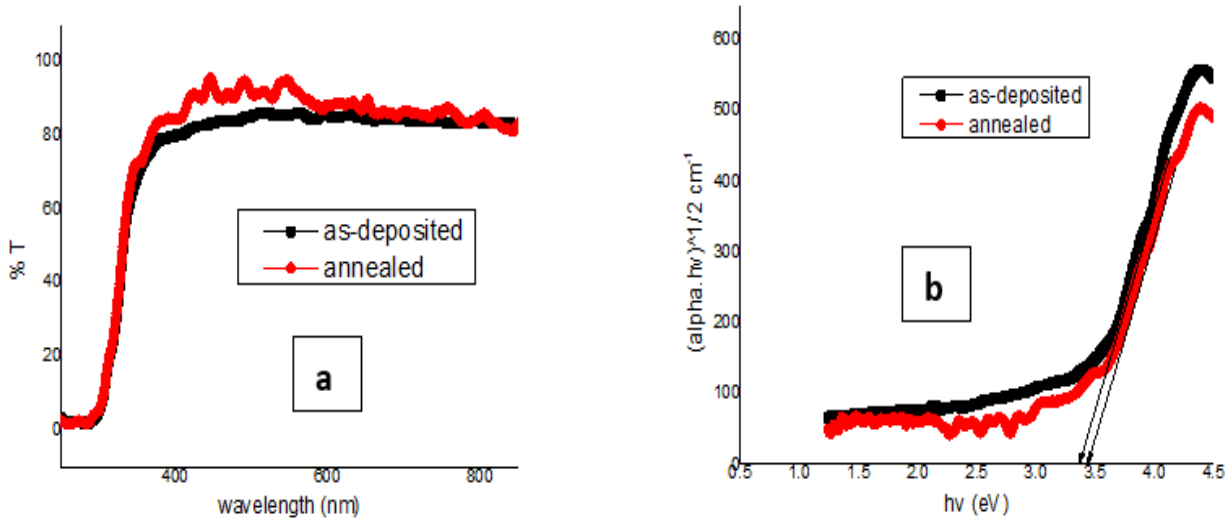

Figure 2: (a) Transmittance and (b) Tauc's plots for optical band gap of as-deposited and annealed SnO_2-CuO Composite films

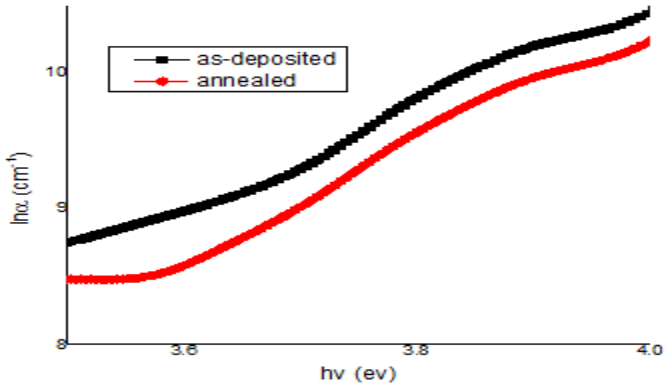

Figure 3: Plot for determination of the Urbach energy E_t.

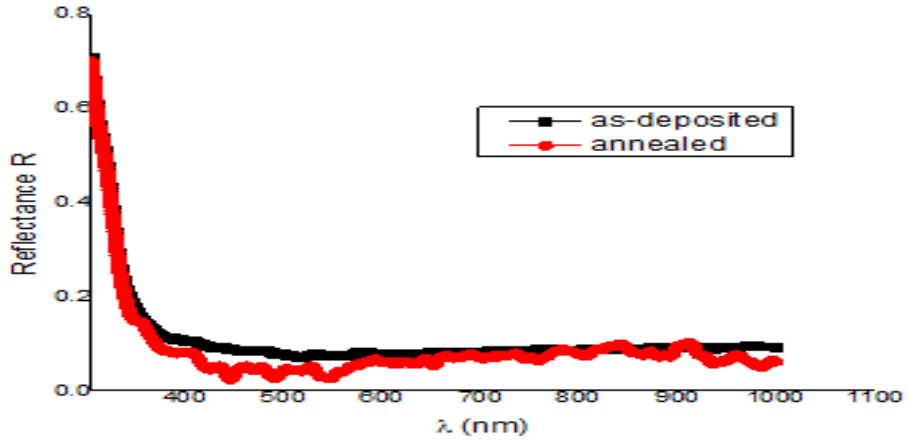

Figure 4: Reflectance against wavelength for as-deposited and annealed films

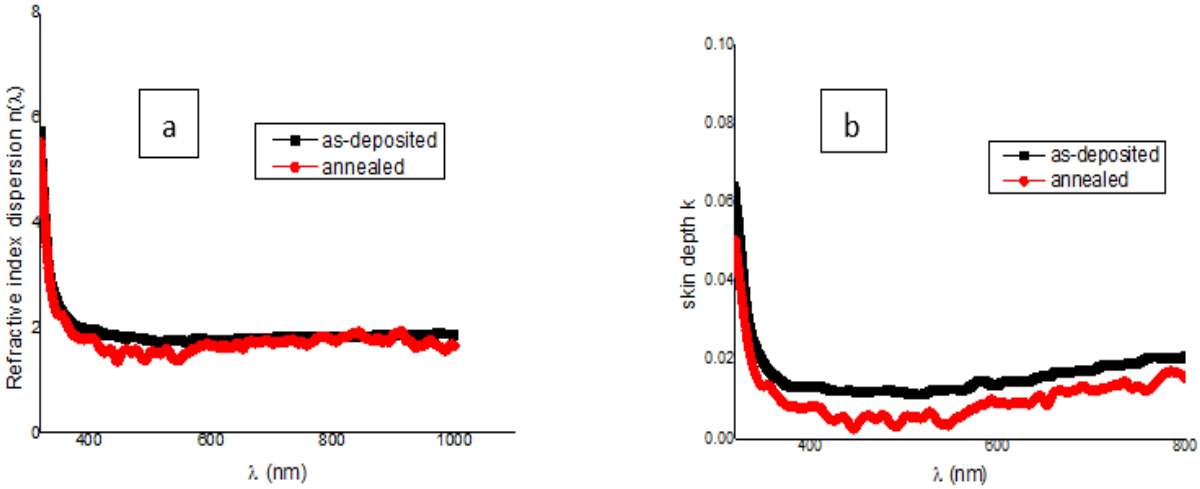

Figure 5: (a) Refractive index and (b) skin depth versus wavelength for as-deposited and annealed films

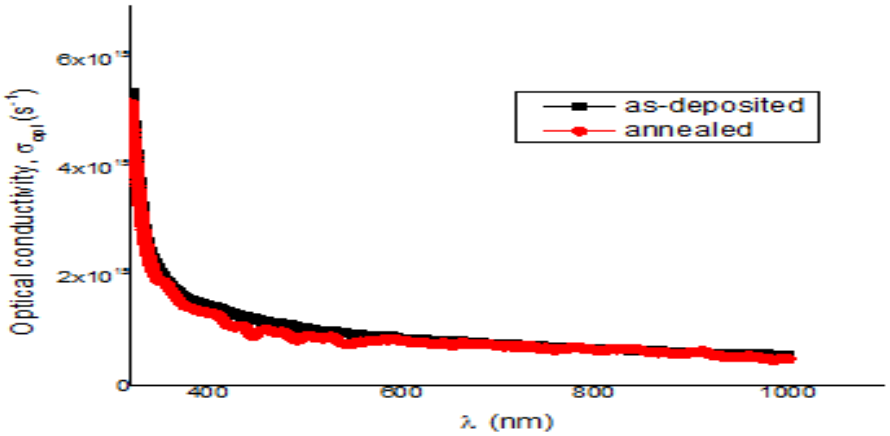

Figure 6: Optical conductivity against wavelength

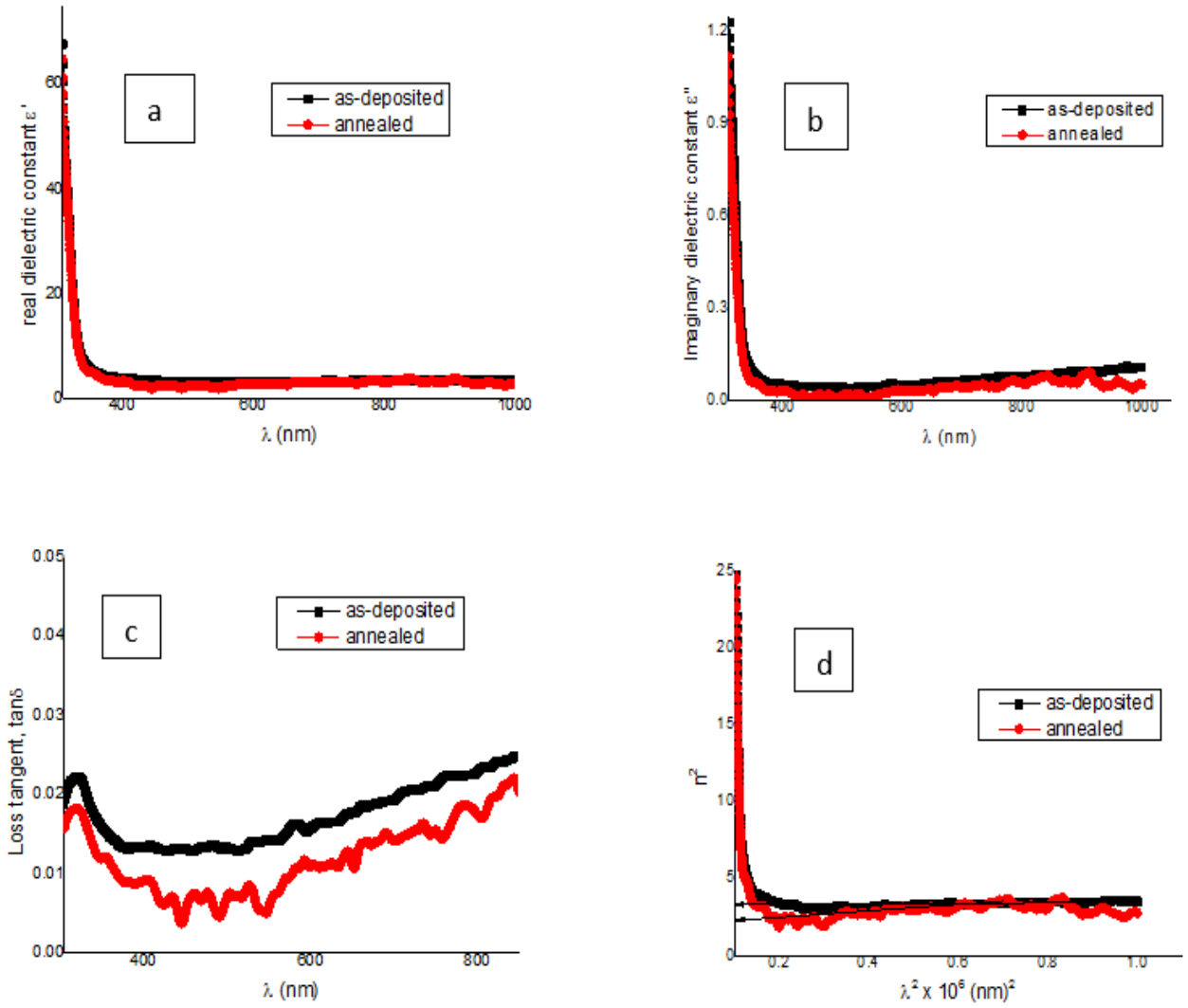

Figure 7: Plots showing the variation of (a) real, (b) imaginary dielectric constants, (c) loss tangent against the wavelength and (d) determination of the high-frequency dielectric constant (ε_α) of as-deposited and annealed films

Discussion

Two important features could be inferred from the RBS analysis. The annealed sets of the same composition increased in thickness compared with the as-deposited sample. This may be ascribed to the familiar behaviour of SnO_2 grains, which grow in size as a result of annealing (Batzil *et al*, 2005) and appears thicker. Besides, it is also evident that there is a slight variation in the Cu^{2+} and O^{2-} compositions. The oxygen composition slightly increased in the annealed film. We attributed this to adsorption of ambient oxygen during annealing since the samples were annealed in an open tubular furnace. However, our simulations showed that both films were stoichiometric in compositions indicating that no new compound might have formed as a result of the heat treatment. These variations in thickness were taken into considerations in our optical analysis. As shown in Figure 2(a), the transmittance graph showed that the annealed sample became a little more transparent with a

small shift in the absorption edge after the heat treatment. This could be attributed to improved crystallization and rearrangement of atoms as a result of heat-induced surface diffusion. This also reflected in the small increase in the bandgap of the annealed sample Figure 2(b). Besides this, it is important to note that the composite films showed a narrower optical band (3.4 eV) compared to our earlier reported pure SnO_2 film (3.86 eV) (Animasahun *et al*., 2019). The significance of this is that the composite film can harvest/absorb more electromagnetic photons than the pure SnO_2. This is important in solar energy conversion, photodegradation and photocatalysis. It is also evident from the Tauc's plot that the annealed film has a slightly higher bandgap which is expected because of its lower absorption and less disordered states since its Urbach energy (252 meV) is lower than for as-deposited film (296 meV) as derived from the analysis of Urbach energy plot in Figure 3. It has been noted that the higher the Urbach energy the more the disordered states and the lower the bandgap (Hassanien and Akl, 2016). Figure 4 showed that the reflectance was around 15 % for 350 nm < λ < 800 nm in the as-deposited film. The value became lower for annealed film over the same range of wavelength. In figure 5, the spectral dependence of refractive indices n(λ) was shown. For both films, R and n spectra could be divided into three regions. The first region where 300 nm < λ < 350 nm which corresponds to UV region presented a rapid change in both reflectance and refractive index and is a region of strong absorption. In the second region where 350 nm < λ < 500 nm, the rate of reduction in both R and n slowed down which also signifies reduced absorption of photons. The third region; λ > 500 nm, R and n plateaued. The rapid change of n and R in the first region could be attributed to the electronic band to band transition (Fasasi *et al.*, 2018) as a result of the high photon energy of the UV light while the slow rate of variation in the second region could as well be ascribed to the lower photon energies of the far UV and the visible light. In the third region, R and n are almost invariant with an increasing wavelength which resulted in little or no absorption of the incident light. These observations followed normal dispersion behaviour. Also, it was observed that refractive indices of the annealed film are a bit lower to the ad-deposited film and in fact lower than the earlier reported value for pure SnO_2 films (Animasahun *et al.*, 2019). This reduction is a further justification for improvement in the atomic arrangement as a result of annealing. The dependence of optical conductivity on photon energy also followed the trend observed in refractive index dispersion. At lower wavelengths and high photon energies, the optical conductivity was very high and decreased as the photon energies were decreasing following the three-region pattern again. This could be explained in terms of excitation of charge carriers – a fundamental behaviour of semiconductors which increase in conductivity as a result of excitations and as long as excitation energy is equal or greater than their band gaps. As shown in figure 7 (a) and (b), the real component ε' of the dielectric complex function is far greater than the imaginary component ε'' for both films. This is expected as ε' depends mostly on refractive index n which is far greater than skin depth k on which the imaginary ε'' depends. Also, the real component ε' for the as-deposited film is a wee greater than for the annealed film. Since ε' is responsible for the slowing down of electromagnetic waves in materials (Fasasi *et al.*, 2009), it then implies that light photon travels slower in the as-deposited and therefore interact more with free charge carriers than in the annealed film. This corroborated the slightly higher optical conductivity observed in the as-deposited film. The nature of the loss tangent plot Figure 7(c) for both films is essentially the same with both showing a narrow peak at 321 nm. This is indicative of the same relaxation mechanisms in both films. In Figure 7(d), the extrapolation of the linear part of the

curve gave the high-frequency dielectric constants ε_∞ for both films. The as-deposited has a value of 3.27 and the annealed has 2.40. As expected, the value of the high-frequency dielectric constant ε_∞, for the as-deposited film is higher than for the annealed film. This followed from their dependence on the value of the refractive index and agrees with the observed trend in the behaviour of both films. It also showed the effect of heat treatment on the behaviour of composite films.

Conclusions

SnO_2-CuO mixed oxides films were deposited on a soda-lime glass substrate via cost-effective and facile chemical spray pyrolysis method. The films were characterized to investigate the effects of CuO on the optical and dielectric properties of SnO_2. The simulations and analysis of the RBS data gave the composition and thickness of the films. The optical band gap decreased from 3.85 for SnO_2 to 3.4 for SnO_2-CuO showing the effect of the presence of CuO. This study also showed that the existence of CuO in the matrix of SnO_2 led to a decrease in its refractive index and dielectric constants. Our investigation led to conclude that the addition of CuO into SnO_2 increased its electromagnetic photon absorption and also reduce its speed thereby enhancing photon interaction with free charge carriers in the mixed oxide film. We opined that the mixed oxide will perform better in photocatalysis, photodegradation of pollutants and other light-harvesting applications.

Conflict of Interest

Authors declare no conflict of interests.

References

Akbar, W., Elahi, I. and Nazir, S. (2020). Development of Ferromagnetism and Formation Energetics in 3d TM-doped SnO_2: GGA and GGA+ U Calculations. *Journal of Magnetism and Magnetic Material*, 5(11): 166948.

Animasahun, L.O., Taleatu, B.A., Bolarinwa, H.S., Fasasi, A.Y., Eleruja, M.A., Obiajunwa E. I. and Pelemo, D. (2019). Spray Pyrolysis Deposition and Characterizations of Dielectric SnO_2 Thin Films. *Fountain Journal of Natural and Applied Sciences,* 8(2): 11-20.

Ayadi, M., Benhaoua, O., Sebais, M., Halimi, O., Boudine, B. and Aida, M. S. (2019). Effect of cerium doping on the structural, optical and photocatalytic properties of SnO_2 thin films prepared by spray pyrolysis method. *Materials Research Express*, *6*(7): 076407.

Babu, B., Kadam, A. N., Ravikumar, R. V. S. S. N. and Byon, C. (2017). Enhanced visible-light photocatalytic activity of Cu-doped SnO_2 quantum dots by solution combustion synthesis. *Journal of Alloys and Compounds*, 703: 330-336.

Batzill, M., and Diebold, U. (2005). The surface and materials science of tin oxide. *Progress in surface science,* 79(2): 47-154.

Bhadane, M. S., Gavhane, K. H., Thorat, A. B., Joshi, R. P., Katre, K. T., Dahiwale, S. S., ... and Dhole, S. D. (2019). Structural, morphological and 6 MeV energy electron dosimetric properties of Cu doped SnO_2 phosphor. *Materials Research Express,* 6(5): 055901.

Brousseau, J. L., Bourque, H., Tessier, A. and Leblanc, R. M. (1997). Electrical properties and the topography of SnO_2 thin films prepared by reactive sputtering. *Applied surface science,* 108(3): 351-358.

Chen, D., Huang, S., Huang, R., Zhang, Q., Le, T. T., Cheng, E., ... and Chen, Z. (2019). Convenient fabrication of Ni-doped SnO2

quantum dots with improved photodegradation performance for Rhodamine B. *Journal of Alloys and Compounds*, 788: 929-935.

Choi, S. W., Katoch, A., Zhang, J. and Kim, S. S. (2013). Electrospun nanofibers of CuO-SnO_2 nanocomposite as semiconductor gas sensors for H_2S detection. *Sensors and Actuators B: Chemical,* 176: 585-591.

Fasasi, A. Y., Ngom, B. D., Kana-Kana, J. B., Bucher, R., Maaza, M., Theron, C. and Buttner, U. (2009). Synthesis and characterisation of Gd-doped BaTiO3 thin films prepared by laser ablation for optoelectronic applications. *Journal of Physics and Chemistry of Solids*, 70(10): 1322-1329.

Fasasi, A. Y., Osagie, E., Pelemo, D., Obiajunwa, E., Ajenifuja, E., Ajao, J., Osinkolu, G., Makinde, W. O. and Adeoye, A. E. (2018). Effect of Precursor Solvents on the Optical Properties of Copper Oxide Thin Films Deposited Using Spray Pyrolysis for Optoelectronic Applications. *American Journal of Materials Synthesis and Processing*, 3(2): 12-22.

Garino, N., Sacco, A., Castellino, M., Muñoz-Tabares, J. A., Chiodini, A., Agostino, V., Margaria, V. Gerosa, M., Massaglia, G. and Quaglio, M. (2016). Microwave-assisted synthesis of reduced graphene oxide/SnO2 nanocomposite for oxygen reduction reaction in microbial fuel cells. *ACS applied materials & interfaces*, 8(7): 4633-4643.

Hassanien, A. S. and Akl, A. A. (2016). Effect of Se addition on optical and electrical properties of chalcogenide CdSSe thin films. *Superlattices and Microstructures*, 89: 153-169.

Jahnavi, V. S., Tripathy, S. K. and Rao, A. R. (2020). Study of the Structural, Optical, Dielectric and Magnetic Properties of Copper-Doped SnO_2 Nanoparticles. *Journal of Electronic Materials,* 49(3):1-15.

Karpuraranjith, M., Chen, Y., Wang, X., Yu, B., Rajaboopathi, S. and Yang, D. (2020). Hexagonal SnSe nanoplate supported SnO2-CNTs nanoarchitecture for enhanced photocatalytic degradation under visible-light-driven. *Applied Surface Science*, 507: 145026.

Letifi, H., Litaiem, Y., Dridi, D., Ammar, S. and Chtourou, R. (2019). Enhanced Photocatalytic Activity of Vanadium-Doped SnO2 Nanoparticles in Rhodamine B Degradation. *Advances in Condensed Matter Physics*. *2019*.

Liu, X., Cheng, S., Liu, H., Hu, S., Zhang, D. and Ning, H. (2012). A survey on gas sensing technology. *Sensors*, 12(7): 9635-9665.

Magdalane, C. M., Kanimozhi, K., Arularasu, M. V., Ramalingam, G. and Kaviyarasu, K. (2019). Self-cleaning mechanism of synthesized SnO_2/TiO_2 nanostructure for photocatalytic activity application for wastewater treatment. *Surfaces and Interfaces,* 17: 100346.

Mahmood, K., Swain, B. S., Kirmani, A. R., and Amassian, A. (2015). Highly efficient perovskite solar cells based on a nanostructured WO_3–TiO_2 core-shell electron transporting material. *Journal of Materials Chemistry A*, 3(17): 9051-9057.

Nachiar, R. A. and Muthukumaran, S. (2019). Structural, photoluminescence and magnetic properties of Cu-doped SnO_2 nanoparticles co-doped with Co. *Optics & Laser Technology*, 112: 458-466

Navidpour, A. H., Fakhrzad, M., Tahari, M. and Abbasi, S. (2019). Novel photocatalytic coatings based on tin oxide

semiconductor. *Surface Engineering*, 35(3): 216-226.

Patil, G. E., Kajale, D. D., Gaikwad, V. B. and Jain, G. H. (2012). Preparation and characterization of SnO2 nanoparticles by hydrothermal route. *International Nano Letters*, 2(1): 1-5.

Sathishkumar, M. and Geethalakshmi, S. (2020). Enhanced photocatalytic and antibacterial activity of Cu: SnO_2 nanoparticles synthesized by microwave-assisted method. *Materials Today: Proceedings*, 20: 54-63.

Shao, T., Liu, S. and Zhang, F. (2019). Electronic structure and optical properties of Cu-doped SnO_2. *Ferroelectrics*, 547(1): 137-147.

Sinatra, L., LaGrow, A. P., Peng, W., Kirmani, A. R., Amassian, A., Idriss, H. and Bakr, O. M. (2015). An $Au/Cu_2O–TiO_2$ system for photocatalytic hydrogen production. A p-n junction effect or a simple case of in situ reduction? *Journal of Catalysis*, 322: 109-117.

Somjaijaroen, N., Sakdanuphab, R. and Sakulkalavek, A. (2019, September). Improved Transparent Gas Sensor Properties of Cu-doped SnO_2 Films using O_2 Plasma Treatment. In *Journal of Physics: Conference Series* (Vol. 1259, No. 1, p. 012022). IOP Publishing.

Sujatha, K., Seethalakshmi, T., Sudha, A. P. and Shanmugasundaram, O. L. (2019). Photocatalytic activity of pure, Zn doped and surfactants assisted Zn doped SnO_2 nanoparticles for degradation of cationic dye. *Nano-Structures & Nano-Objects*, 18: 100305.

Tsay, C. Y., & Liang, S. C. (2015). Fabrication of p-type conductivity in SnO_2 thin films through Ga doping. *Journal of Alloys and Compounds*, 622: 644-650.

Uddin, M. T., Nicolas, Y., Olivier, C., Toupance, T., Servant, L., Müller, M. M., ... and Jaegermann, W. (2012). Nanostructured SnO_2–ZnO heterojunction photocatalysts showing enhanced photocatalytic activity for the degradation of organic dyes. *Inorganic chemistry*, 51(14): 7764-7773.

Ullah, I., Munir, A., Muhammad, S., Ali, S., Khalid, N., Zubair, M. and Hussain, I. (2020). Influence of W-doping on the optical and electrical properties of SnO2 towards photocatalytic detoxification and electrocatalytic water splitting. *Journal of Alloys and Compounds,* 827: 154247.

Yıldırım, M. A., Yıldırım, S. T., Sakar, E. F. and Ateş, A. (2014). Synthesis, characterization of dielectric properties of SnO_2 thin films. *Spectrochimica Acta Part A: Molecular and Biomolecular Spectroscopy*, 133: 60-65.

Yu, Y., Yao, B., Cao, B. and Ma, W. (2019). Morphology-controlled Fabrication of SnO_2/ZnO Nanocomposites with Enhanced Photocatalytic Performance. *Photochemistry and photobiology*, *95*(5): 1131-1141.

Yu-Cheng, C., and Yu-Wen, L. (2020). MoS2@ SnO_2 core-shell sub-microspheres for highly efficient visible-light photodegradation and photocatalytic hydrogen production. *Materials Research Bulletin*, 110912.